# Gyrokinetic microinstability analysis of high-$T_\mathrm{i}$ and high-$T_\mathrm{e}$ isotope plasmas in Large Helical Device

**Motoki Nakata[1,2], Kenichi Nagaoka[1,3], Kenji Tanaka[1], Hiromi Takahashi[1,2], Masanori Nunami[1,2], Shinsuke Satake[1,2], Masayuki Yokoyama[1,2], Felix Warmer[4], and the LHD Experiment Group**

[1] National Institute for Fusion Science, National Institutes of Natural Sciences, Toki 509-5292, Japan
[2] SOKENDAI (The Graduate University for Advanced Studies), Toki 509-5292, Japan
[3] Graduate School of Science, Nagoya University, Nagoya 464-8602, Japan
[4] Max-Planck Institute for Plasma Physics, Greifswald, D-17491, Germany

E-mail: nakata.motoki@nifs.ac.jp

**Abstract.** Transport and confinement characteristics, and microinstabilities for high-$T_\mathrm{i}/T_\mathrm{e}$ and high-$T_\mathrm{e}/T_\mathrm{i}$ isotope plasmas in Large Helical Device are explored by using the gyrokinetic Vlasov simulation GKV with hydrogen isotope ions and real-mass kinetic electrons. The experimental data indicate that the thermal diffusivity is reduced in the deuterium-dominated plasmas, where the deviation from the gyro-Bohm scaling in the overall tendency and the strong anomaly of the electron heat transport are identified. Linear gyrokinetic analyses identify that the growth rates of the ion temperature gradient(ITG) and trapped electron mode(TEM) instabilities in the deuterium plasmas are reduced due to the change in the profile gradients and/or the isotope ion mass, and the radial dependence of the mixing-length diffusivity is qualitatively consistent with the experimental tendency. Also, TEM-like turbulent fluctuations are examined by the using the phase contrast imaging(PCI) measurement and the linear gyrokinetic calculation for the high-$T_\mathrm{e}/T_\mathrm{i}$ deuterium plasma.

## 1. Introduction

Understanding the isotope ion mass effects on transport and confinement in magnetically confined toroidal plasmas is one of the most important issues for realizing self-ignited burning plasmas. There are many experimental evidences [see e.g., Refs. [1, 2, 3]] that the energy confinement time in the case with heavier isotope ions is much improved beyond the estimation of the gyro-Bohm scaling with the ion mass dependence of $m_\mathrm{i}^{1/2}$. However, the physical mechanisms and their interrelationship behind the improved confinement are still remained open.

In our previous theoretical works with gyrokinetic simulations[4, 5], a fundamental physics of the isotope effects on the ion temperature gradient(ITG) and the trapped electron mode(TEM) instabilities has been clarified, as well as their turbulent transport properties and the zonal flow generation. The particular importance is that there exists the significant isotope

mass impacts on the collisional stabilization of the TEM instability, which is expected to be destabilized in tokamak and helical plasmas with the strong electron heating.

Concurrently, the first deuterium plasma experiments in Large Helical Device(LHD) have been conducted in order to make the plasma performance higher, and to explore the physical origin of the isotope effects, where the operation regime has been successfully extended with the remarkable achievement of 10keV for the ion temperature on the axis[6, 7]. In addition to the high-$T_i$ discharges with the neutral beam injection(NBI) heating, an improved confinement in the deuterium plasma is observed in the high-$T_e$ discharges with electron cyclotron resonance heating(ECRH)[7, 8]. For their comprehensive understandings, the joint analyses of experiments and gyrokinetic simulations are indispensable.

In this study, transport and confinement characteristics, and microinstabilities for the high-$T_i/T_e$ and high-$T_e/T_i$ isotope plasmas in LHD are investigated by using the gyrokinetic Vlasov simulation GKV with hydrogen isotope ions and real-mass kinetic electrons[12, 13]. Then, the qualitative features among the cases for the hydrogen, deuterium, high-$T_i$, and high-$T_e$ plasmas are identified.

The rest of the paper is organized as follows. The experimental results in LHD isotope plasmas are presented in Sec. 2. Then, the results of gyrokinetic microinstability analyses using the experimental conditions are shown in Sec. 3. In Sec. 4, the comparison between the fluctuation measurement and linear gyrokinetic calculation for the TEM instability is discussed. Finally, the concluding remarks are given in Sec. 5.

## 2. NBI-sustained and ECRH-sustained isotope plasma experiments

Experimental results for the high-$T_i/T_e$ and high-$T_e/T_i$ isotope plasmas in LHD, which are used for the present linear gyrokinetic calculation, are shown in this section, where the NBI and ECRH are mainly utilized to produce the high-$T_i/T_e$ and high-$T_e/T_i$ plasmas, respectively. The details about the typical experimental setups for NBI- and ECRH-sustained plasmas are shown in, e.g., Refs. [14, 15, 16, 7, 8].

The kinetic profiles for the high-$T_i/T_e$ plasmas are shown in Figs. 1(a) – 1(c), where the Thomson scattering(TS) system[9] and the charge exchange spectroscopy(CXS)[10] are used for the measurements of $T_e$-, $n_e$-, and $T_i$-profiles, respectively. Here we compare the hydrogen-dominated case of LHD #132031 at $t = 3.74$sec (labeled by "H: #132031t3740") with $n_H(\rho = 0)/n_e(\rho = 0) = 0.84$, and the deuterium-dominated case of LHD #139727 at $t = 4.37$sec (labeled by "D: #139727t4370") with $n_D(\rho = 0)/n_e(\rho = 0) = 0.87$. The magnetic field intensity and the averaged major radius at the magnetic axis in the vacuum field are given by $\{B_{ax}^{(vac)} = -2.75\text{T}, R_{ax}^{(vac)} = 3.60\text{m}\}$ and $\{B_{ax}^{(vac)} = -2.85\text{T}, R_{ax}^{(vac)} = 3.60\text{m}\}$ for the H- and D-plasmas, respectively. The total port-through NBI power is 21.4MW for the H-plasma, and is 20.5MW for the D-plasma. The normalized logarithmic gradients $R_{ax}/L_X := -(R_{ax}/a)d\ln X/d\rho$ for $X = \{T_i,\ T_e,\ n_e\}$ are shown in Figs. 1(d) – 1(f), where the temperature and density profiles are polynomially interpolated with the measurement data for both the inboard and outboard sides, and the finite-$\beta$ Shafranov shift is included in the major radius at the magnetic axis $R_{ax}$. We see that the D-plasma indicates a relatively higher $T_i$ and

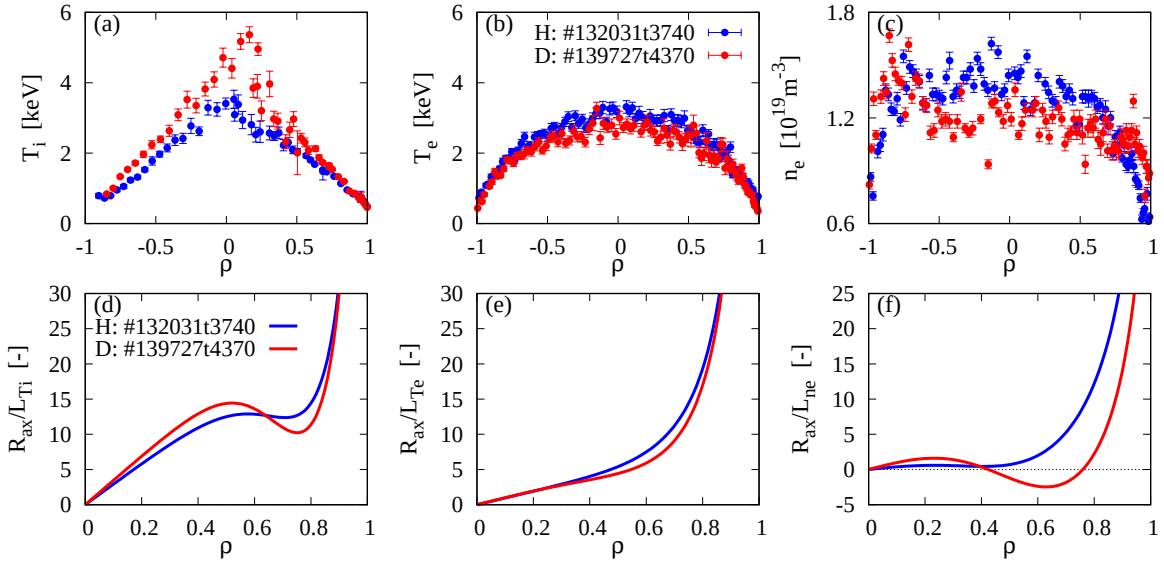


**Figure 1.** Radial profiles of (a)the ion temperature, (b)the electron temperature, (c)the electron density, and [(d) – (f)]their logarithmic gradients $R_{ax}/L_{T_i}$, $R_{ax}/L_{T_e}$, and $R_{ax}/L_{n_e}$ in the LHD high-$T_i/T_e$ plasmas with the hydrogen (H: #132023t3740) and the deuterium (D: #139727t4370).

relatively more hollow $n_e$ profile, where the global energy confinement time is evaluated as $\tau_E$ = {22.5msec(H), 24.3msec(D)}, indicating 8% improvement in the D-plasma.

Figures 2(a) – 2(e) display the kinetic profiles and their logarithmic gradients for the high-$T_e/T_i$ plasmas, where the hydrogen-dominated case of LHD #143742 at $t$ = 5.40sec (labeled by "H: #143742t5400") and the deuterium-dominated case of LHD #139080 at $t$ = 4.97sec (labeled by "D: #139080t4970") are compared. The magnetic field intensity and the averaged major radius at the magnetic axis in the vacuum field are given by $\{B_{ax}^{(vac)} = +2.75\text{T}$, $R_{ax}^{(vac)} = 3.60\text{m}\}$ for both the H- and D-plasmas. Note that the profile data in Figs. 2 are time-averaged for the subsequent 100msec, and the electron density profiles are measured by FIR interferometer system[11]. The total port-through ECRH power is fixed with 3.5MW for both the H- and D-plasma cases. Although the difference of $T_e$ and $T_i$ is only slight, more hollow $n_e$ profile is observed in the D-plasma, which is similar to the high-$T_i/T_e$ cases. The global energy confinement time is evaluated as $\tau_E$ = {11.4msec(H), 12.7msec(D)}, indicating 11.4% improvement in the D-plasma. Note that since the particle source is highly localized near the edge region of $\rho \sim 1$ for the present ECRH-sustained plasmas, the externally injected particle flux is negligible in the core region.

The transport and confinement characteristics are compared between the H- and D-plasmas, where the radial profiles of the ion and electron thermal diffusivities, $\chi_i$ and $\chi_e$, evaluated from the experimental power balance are shown in Figs. 3(a) – 3(d). The thermal diffusivity normalized by the gyro-Bohm diffusivity, $\chi_{GB(s)} = 2^{3/2}\rho_{ts}^2 v_{ts}/R_{ax}$ for s={H, D}, is also plotted in the figures, where the thermal gyroradius and the thermal speed are defined as $\rho_{ts} := m_s v_{ts}/e_s B_{ax}$ and $v_{ts} := (T_s/m_s)^{1/2}$, respectively.

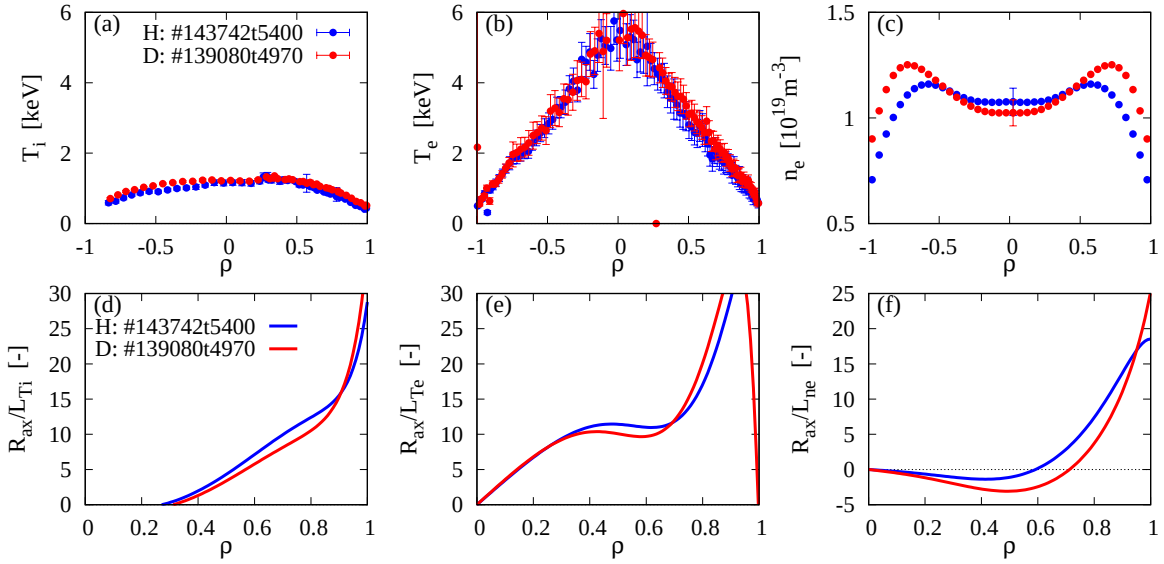


**Figure 2.** Radial profiles similar to those in Figs. 1, but for the LHD high-$T_e/T_i$ plasmas with the hydrogen (H: #143742t5400) and the deuterium (D: #139080t4970).

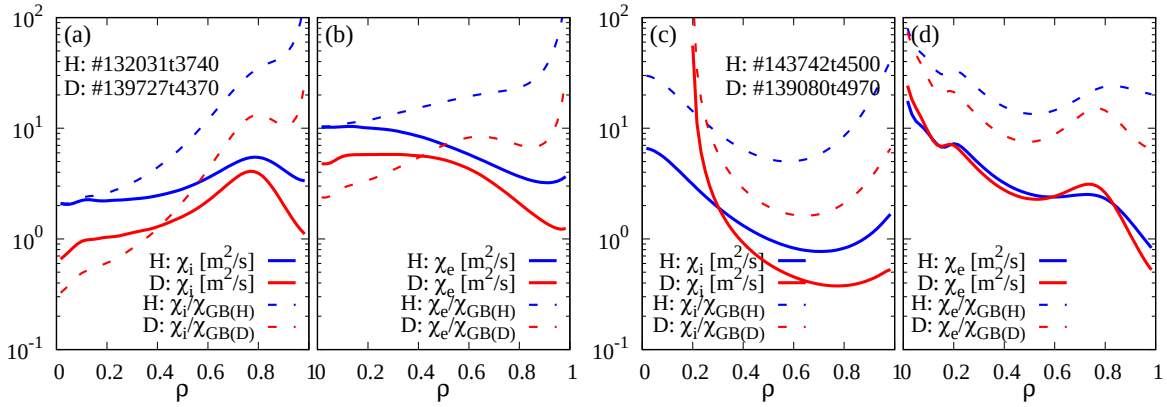


**Figure 3.** Radial profiles of the thermal diffusivity $\chi$ for [(a), (b)]ions and electrons in the high-$T_i/T_e$ isotope plasmas, and for [(c), (d)]those in the high-$T_e/T_i$ cases, where the results are obtained from the experimental power balance. The profiles normalized by the gyro-Bohm diffusivity are also plotted for comparisons.

It is clearly observed in Figs. 3 that $\chi_i/\chi_{GB(D)}$ is reduced in the D-plasma for both the high-$T_i/T_e$ and high-$T_e/T_i$ cases. Ideally, $\chi_i/\chi_{GB(D)}$ in the D-plasma must coincide with $\chi_i/\chi_{GB(H)}$ in the H-plasma if the transport property is, completely, of the gyro-Bohm scaling. However, it should be noted here that the changes in the density profiles, temperature profiles, and the radial electric fields have impact on the confinement performance. This will be discussed in Sec. 3. One also finds the strong anomaly of the electron heat transport, i.e., $\chi_e \sim \chi_i$, for both the high-$T_i/T_e$ and high-$T_e/T_i$ cases. This implies the significant deviation from the gyro-Bohm argument for the electron thermal diffusivity.

## 3. Linear gyrokinetic calculations for LHD isotope plasmas

In the previous section, the improved confinement is discussed for the high-$T_i/T_e$ and high-$T_e/T_i$ isotope plasmas in LHD. Since, in experiments, the kinetic profiles simultaneously varies with the isotope ion species, the microinstability analysis with the realistic experimental condition is essential to identify separately the profile effects and the isotope ion mass effects.

To this end, the linear gyrokinetic calculations are carried out by using GKV, the multi-species electromagnetic gyrokinetic Vlasov simulation code (see, e.g., Refs. [12, 13]), for the high-$T_i/T_e$ and high-$T_e/T_i$ LHD plasmas. The hydrogen isotope ions and real-mass kinetic electrons are treated simultaneously, including the collisional effects. Although the electromagnetic effects are included, the magnitude of the magnetic fluctuations is negligibly small due to the low-$\beta$ values for the plasmas of interest. Note that the finite $\rho^*$ and the impurity effects, such as the mean-$E_r$ shear and the charge density dilution for the main ion, are ignored in the present calculations. More details of the simulation model in GKV for the three-dimensional helical plasmas are given in Ref. [4].

Figures 4(a) – 4(c) show the poloidal wavenumber spectra of the linear growth rate, $\gamma(k_y)$, at several radial positions in the high-$T_i/T_e$ plasmas, where the symbols in the figure mean that the eigenmode is dominated by ITG or TEM. The common normalization factor with the hydrogen thermal speed is used for $\gamma$ to compare the magnitude between the H- and D-plasmas. As expected from the logarithmic gradient profiles shown in Figs. 1(d) – 1(f), the ITG instability dominates the core region of $\rho \leqslant 0.7$. In contrast, the outer core region is dominated by the TEM instability, which is destabilized by both the electron temperature gradient and the density gradient. It is also found that the growth rate in the D-plasma is lower than that in the H-plasma, regardless of the dominant microinstability. As clarified in Ref. [5], the collisional stabilization of the TEM instability is enhanced by the isotope ion mass, while there is little impact of the ion mass on the ITG instability for the case without the mean-$E_r$ shear effects[17]. Hence, the reduction in the ITG growth rate is mainly associated with the profile effects, i.e., theoretically the decreases of $R_{ax}/L_{n_e}$ and $T_e/T_i$ can stabilize the ITG instability. As for the TEM instability at $\rho = 0.9$, both the isotope mass and the profile effects lead to the significant stabilization.

The wavenumber spectra of the linear growth rate in the high-$T_e/T_i$ cases are shown in Figs. 4(d) – 4(f). It is stressed that, in contrast to the high-$T_i/T_e$ cases, the TEM-dominated state with the collisional isotope effects appears in the very core($\rho$ = 0.36) and the outer core($\rho$ = 0.9) regions. In some cases, we also observe the destabilization of the electron temperature gradient(ETG) instability.

In order to make a qualitative comparison between the experimental power balance and the linear gyrokinetic calculations, the mixing-length diffusivity $\chi_{ML}$ is evaluated from the wavenumber spectra of the growth rate, where $\chi_{ML} := \sum_{k_y}(\gamma/k_y^2)\overline{\Delta k_y}$ for $k_r = 0$, and $\overline{\Delta k_y}$ denotes the non-dimensional minimum grid size in $k_y$. Figures 5(a) and 5(b) show the radial dependence of $\chi_{ML}/\chi_{GB}$ for the high-$T_i/T_e$ and high-$T_e/T_i$ isotope plasmas, respectively. One finds the qualitatively consistent results in comparison with Figs. 3 that the gyro-Bohm normalized thermal diffusivity is reduced in the D-plasmas. For the quantitative comparisons

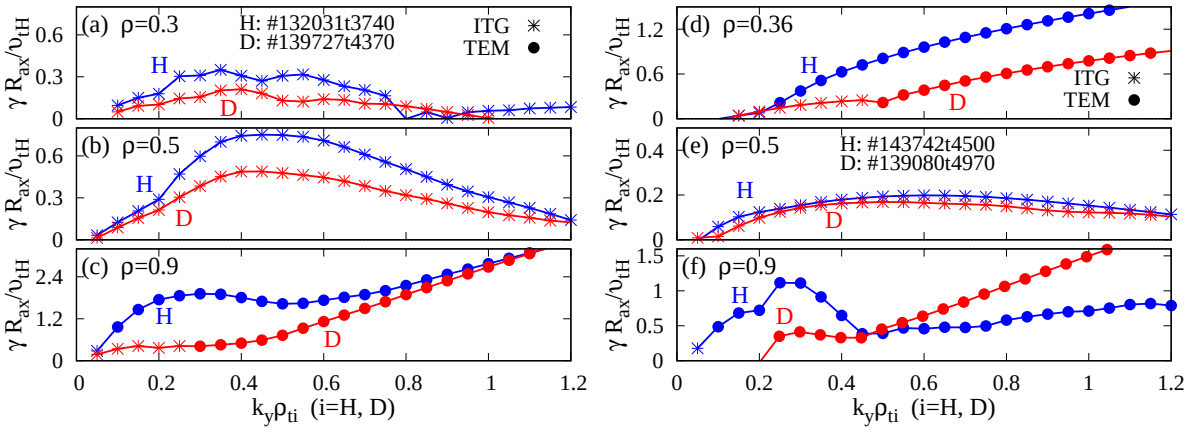


**Figure 4.** Poloidal wavenumber spectra of the linear growth rate at (a)$\rho = 0.3$, (b)$\rho = 0.5$, and (c)$\rho = 0.9$ for the high-$T_i/T_e$ isotope plasmas, and at (d)$\rho = 0.36$, (e)$\rho = 0.5$, and (f)$\rho = 0.9$ for the high-$T_e/T_i$ cases. The most unstable modes with $k_r = 0$ are plotted.

including the separate evaluation of $\chi_i$ and $\chi_e$, one needs the nonlinear turbulence simulations, which will be addressed in the future work.

The reduction of $\chi_{ML}$ results from the change in the profile gradients and/or the isotope ion mass. As shown in Fig. 5(c), the above point is more clearly examined by the specific parameter scans with respect to the electron density gradient, where the dependence of $\gamma$ on $R_{ax}/L_{n_e}$ is plotted for the ITG and TEM cases. For comparison, the results for the cases with the inward-shifted magnetic configuration are also shown in the figure. One can see that the decrease in $R_{ax}/L_{n_e}$ towards the negative value leads to stabilization of both the ITG and TEM instabilities. Even though the inward-shifted cases show larger growth rates due to the changes in the magnetic drift, etc., $R_{ax}/L_{n_e}$-dependence is quite similar to that in the standard configuration cases. It is also noted that the $R_{ax}/L_{n_e}$-stabilization of the TEM instability is more significant than that of the ITG case.

In experimental results shown in Figs. 1 and 2, we observed that a more hollow density profile is formed in the D-plasma in comparison to that in the H-plasma. These results suggest that there can be indirect isotope effects on the thermal confinement through the isotope ion mass impacts on the particle transport leading to $R_{ax}/L_{n_e}$-stabilization for the ITG and TEM instabilities. The isotope effects on the particle transport should be addressed by means of the nonlinear gyrokinetic simulations, as well as dedicated experiments with precise control of the external particle source.

## 4. Identification of TEM-like turbulent fluctuations

The transport and confinement characteristics in LHD isotope plasmas are discussed in the previous sections. In addition, elucidating the isotope ion mass impacts on the turbulent fluctuations is a critical issue from both the theoretical and the experimental points of view. So far, the comparison between the gyrokinetic calculations and the fluctuation measurements

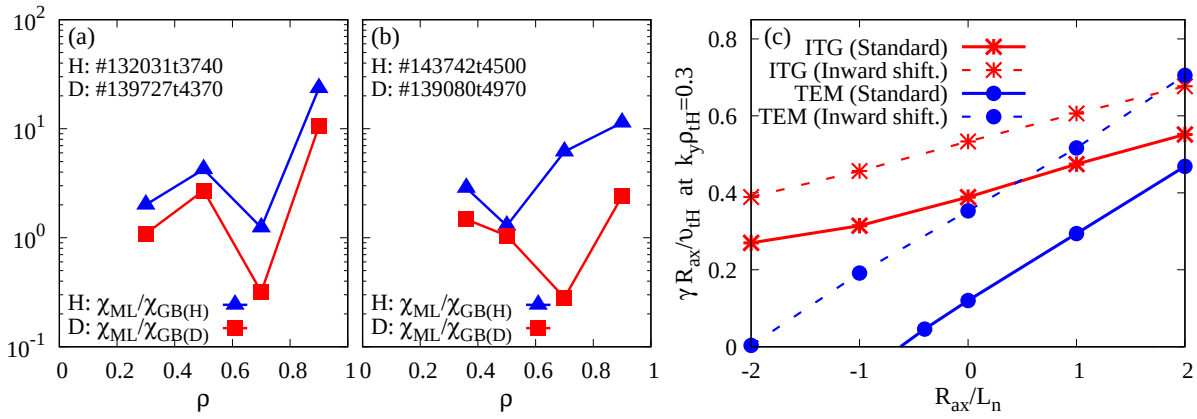


**Figure 5.** Radial dependence of the mixing-length diffusivity $\chi_{ML}/\chi_{GB}$ for (a)the high-$T_i/T_e$ and (b)the high-$T_e/T_i$ isotope plasmas. (c)dependence of $\gamma(k_y\rho_{tH} = 0.3)$ on the electron density gradient $R_{ax}/L_{n_e}$ (from hollow to peaked) in the ITG and TEM cases, where the results of the inward shifted magnetic configuration($R_{ax}^{(vac)} = 3.60$m) are also plotted for comparison with the standard configuration cases($R_{ax}^{(vac)} = 3.75$m).

using the phase contrast imaging(PCI)[18, 19] has extensively been carried out for the ITG cases in LHD[20, 21, 22, 23].

In this work, TEM-like fluctuations observed in the high-$T_e/T_i$ deuterium plasma are discussed. The experimental results from the PCI measurement is shown in Fig. 6(a), where the fluctuation intensity is plotted as a function of the radial position and phase velocity in the laboratory frame. Note that the profile conditions of the experimental data of #139079, which is used here, are qualitatively similar to those in the deuterium case shown in Figs. 2. Also, the poloidal rotation velocity due to the mean-$E_r$ formation is evaluated from the heavy ion beam probe(HIBP) and the charge exchange spectroscopy(CXS), and is over-plotted in the figure. One finds that the high intensity region with the phase velocity of 3km/s is spread over $0.4 \leqslant \rho \leqslant 0.8$, where $k_\perp \rho_{tD} \sim 0.4$ is identified. It is emphasized that the ion-gyroradius-scale fluctuations with the phase velocity in the electron diamagnetic direction on the co-moving frame with respect to the mean poloidal rotation suggest the TEM-like characteristics. In fact, although the radial position is slightly shifted, the destabilization of the TEM instability is demonstrated by linear gyrokinetic calculations, as shown in Fig. 6(b). Since the recent work on the nonlinear TEM simulation for a quasi-helical-symmetry stellarator indicates the flip of the phase velocity in the nonlinear phase[24], further systematic comparisons between the experiments and the simulations are required, and will be reported elsewhere.

## 5. Concluding remarks

In this study, transport and confinement characteristics, and microinstabilities for the high-$T_i/T_e$ and high-$T_e/T_i$ isotope plasmas in LHD are investigated by using the gyrokinetic Vlasov simulation GKV with hydrogen isotope ions and real-mass kinetic electrons. The experimental data for both the high-$T_i/T_e$ and high-$T_e/T_i$ cases clearly indicate that the gyro-

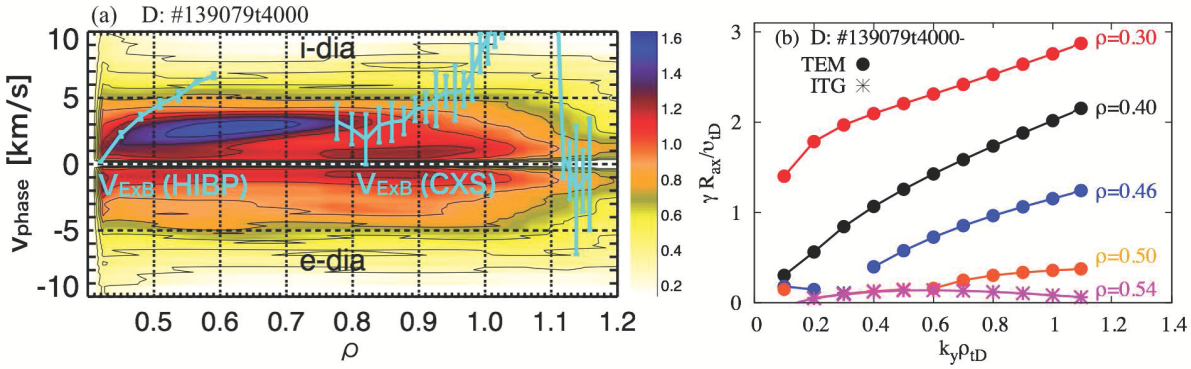


**Figure 6.** (a)fluctuation intensity obtained from PCI measurement for the high-$T_e/T_i$ deuterium plasma and the poloidal rotation velocity due to the mean-$E_r$ formation measured by HIBP and CXS. (b)Wavenumber spectra of the mode growth rate obtained from the linear gyrokinetic calculations.

Bohm normalized thermal diffusivity is reduced in the deuterium-dominated plasmas. The deviation from the gyro-Bohm scaling in the overall tendency and the strong anomaly of the electron heat transport are identified.

Linear gyrokinetic analyses using the realistic experimental conditions identify that the ITG and TEM instabilities dominate the core and edge regions, respectively, in the high-$T_i/T_e$ plasmas, while the TEM-dominated state is also found at the very core region in the high-$T_e/T_i$ cases. It is found that the growth rate in the deuterium plasmas is reduced due to the change in the profile gradients and/or the isotope ion mass, and the radial dependence of the mixing-length diffusivity is qualitatively consistent with the experimental tendency.

Furthermore, the turbulent fluctuation characteristics observed with PCI measurement in the high-$T_e/T_i$ deuterium plasma are compared with the linear gyrokinetic calculations. The ion-gyroradius-scale fluctuations with the phase velocity in the electron diamagnetic direction on the rest frame with respect to the mean poloidal rotation suggest the TEM-like characteristics, which are qualitatively consistent with the TEM instability evaluated by gyrokinetic simulations.

## Acknowledgments

The authors would like to thank Drs. H. Sugama, T. -H. Watanabe, S. Toda, and C. Hidalgo for fruitful discussions on this study. Numerical simulations were performed by Plasma Simulator at NIFS, and by FX100 at Nagoya University. This work is supported by the MEXT Japan, Grant No. 17K14899, in part by the NIFS collaborative Research Programs, and in part by the MEXT grant for Post-K project: Development of Innovative Clean Energy, Core Design of Fusion Reactor.

## References

[1] M. Bessenrodt-Weberparl *et al.*, Nucl. Fusion 33, 1205 (1993)

[2] H. Urano *et al*., Phys. Rev. Lett. 109, 125001 (2012)
[3] U. Stroth *et al*., Physica Scripta 51, 655 (1995)
[4] M. Nakata *et al*., Plasma Phys. Control. Fusion 58, 074008 (2016)
[5] M. Nakata *et al*., Phys. Rev. Lett. 118, 165002 (2017)
[6] Y. Takeiri *et al*., Nucl. Fusion 57, 102023 (2017)
[7] H. Takahashi *et al*., submitted to Nucl. Fusion
[8] F. Warmer *et al*., submitted to Nucl. Fusion
[9] I. Yamada *et al*., Fusion Sci. Tech. 58, 345 (2010)
[10] M. Yoshinuma *et al*., Fusion Sci. Tech. 58, 375 (2010)
[11] K. Tanaka *et al*., Plasma Fusion Res. 3, 050 (2008)
[12] T. -H. Watanabe *et al*., Nucl. Fusion 46, 24 (2006)
[13] M. Nakata *et al*., Comput. Phys. Commun. 197, 61 (2015)
[14] K. Nagaoka *et al*., Nucl. Fusion 55, 113020 (2015)
[15] K. Tanaka *et al*., Nucl. Fusion 57, 116005 (2017)
[16] H. Takahashi *et al*., Phys. Plasmas 21, 061506 (2014)
[17] H. Sugama *et al*., Phys. Plasmas 16, 056101 (2009)
[18] K. Tanaka *et al*., Rev. Sci. Instrum. 79, 10E702 (2008)
[19] C. Michael *et al*., Rev. Sci. Instrum. 86, 093503 (2015)
[20] M. Nunami *et al*., Plasma Fusion Res. 6, 1403001 (2011)
[21] M. Nunami *et al*., Phys. Plasmas 20, 092307 (2013)
[22] M. Nunami *et al*., Plasma Fusion Res. 5, S2053 (2010)
[23] A. Ishizawa *et al*., Nucl. Fusion 55, 043024 (2015)
[24] M. J. Pueschel *et al*., Phys. Rev. Lett. 116, 085001 (2016)